DGNSS Ranging for CubeSat Rendezvous and Docking Manoeuvres at LEO

DGNSS Ranging for CubeSat Rendezvous and Docking Manoeuvres at LEO

Alex Minetto*, Giorgio Ammirante†, Fabrizio Stesina†, Fabio Dovis* and Sabrina Corpino†
*Department of Electronics and Telecommunications
†Department of Mechanics and Aerospace Engineering
Politecnico di Torino, Turin, Italy
Email: name.surname@polito.it

***Abstract*—In the last decade, the expansion of the Terrestrial Service Volume (TSV) of Global Navigation Satellite Systems (GNSS) toward Medium-Earth Orbits (MEO) is gaining momentum. Low-Earth orbit (LEO) missions have investigated the quality of the GNSS observables, thus demonstrating its availability in near-Earth space. A timely case study is investigated in this work, where a CubeSat is expected to dock a LEO spacecraft while accurately tracking its baseline vector from the object. The mission scenario constitutes a unique chance for the characterization of differential GNSS measurements and the assessment of low-complexity relative GNSS algorithms oriented to collaborative navigation and Positioning, Navigation, and Timing autonomy in space. The paper analyses the simulation results for GNSS-based inter-spacecraft ranging (ISR) measurements leveraging differential, GPS, and Galileo measurements exchanged between the chaser and its mothership. Parametric results analyze the usability of ISRs in rendezvous and docking manoeuvres at LEO altitudes, by comparing their accuracy to pre-defined mission requirements. Output accuracy and precision bounds are eventually provided for the potential integration of ISR into hybrid navigation algorithms.**

***Index Terms*—Global Navigation Satellite Systems (GNSS), Low Earth Orbit (LEO), Differential GNSS, Guidance Navigation and Control**

I. Introduction

Nowadays, a growing effort is paid to extend the use of Global Navigation Satellite System (GNSS) to the Space Service Volume (SSV) as a way to provide positioning and timing services beyond the Terrestrial Service Volume (TSV) [1]. TSV already includes low Medium-Earth Orbits (MEO) and with this transient, modern GNSS have already proved to be usable in near-Earth space where Low-Earth Orbit (LEO) missions have contextually assessed the quality of GNSS measurements [2]. Currently, an increasing number of LEO missions successfully exploit GNSS to perform Orbit Determination and Time Synchronization (ODTS), while modern Guidance, Navigation, and Control (GNC) solutions aim at supporting increased autonomy within and beyond LEO altitudes [3]–[5]. In this paper, we address the application of GNSS-based ranging for automated spacecraft manoeuvres, in particular focusing on Rendezvous and Docking (RVD) phases that are required in most space operations involving multiple probes [5], [6]. Besides direct optical and radiofrequency can cope with this task [7], GNSS-based relative navigation was assessed for the Gravity Recovery and Climate Experiment (GRACE) mission and other programmes up to millimeter-level accuracy through phase ambiguity resolution and advanced Bayesian estimation algorithms [2], [8]–[10]. However, Differential GNSS (DGNSS) techniques may represent a valuable and lower-complexity tool to autonomously navigate the chaser towards the target during the phases of a space rendezvous. In the context of RVD manouvers, DGNSS methods can provide relative state estimates to be integrated with complementary sources of relative navigation data (i.e., relative attitude and angular velocity). In such a context, this contribution proposes a parametric performance analysis for the Inter-Spacecraft Ranging (ISR) performed by a pair of approaching LEO spacecrafts, leveraging fundamental GNSS-based relative navigation techniques. The study aims at assessing the theoretical feasibility of such an approach and to characterize ISRs statistical properties. This aims in turn at supporting ISR integrations in the core Guidance, Navigation and Control (GNC) algorihms for the relative navigation of the CubeSat, under the realistic Absolute Knowledge Error (AKE) requirements. The simulated scenario is inspired by the Space Rider Observer Cube (SROC) mission, which aims at demonstrating the critical capabilities and technologies required for successfully executing an RVD mission of a CubeSat in a safety-sensitive context [11]. The study characterises differential GNSS measurements and assesses their applicability to low-complexity, relative GNSS algorithms and onboard sensor fusion solutions [12]. In particular, the investigated algorithms leverage the maximum likelihood estimation of the ISR using single or double differences of GNSS, carrier-smoothed pseudorange measurements.

The remainder of this paper is structured as follows. Section II introduces differential GNSS algorithms investigated in the study. Section III presents the statistical results of the ISR estimation across the rendezvous phases of the mission. Eventually, conclusions are drawn in Section IV.

II. Methodology

The aim of relative GNSS in the investigated scenario is to estimate the Euclidean distance between the approaching

The study was conducted under ESA contract no. 4000136625/21/NL/MG in the GSTP framework supported by ASI. The authors wish to thank all the members of the SROC team at Politecnico di Torino, Tyvak International and Università di Padova who contributed to the development of the study, together with the experts of the ESA's team that supported the activity.

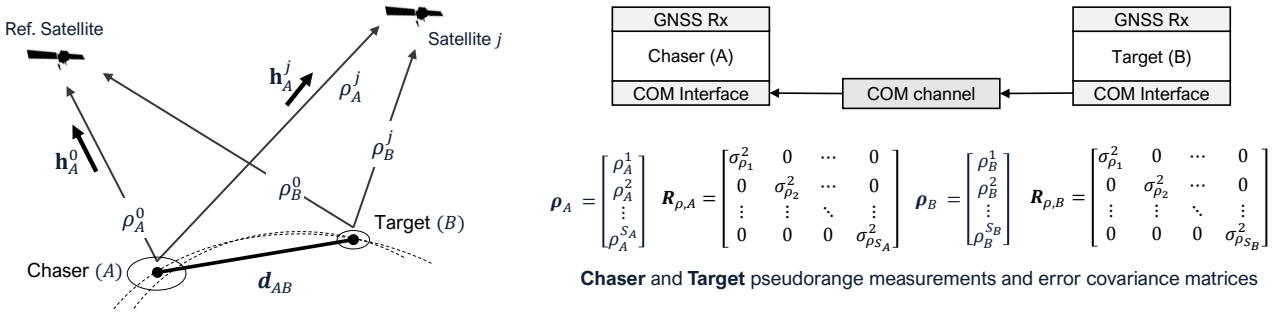

Fig. 1: Geometrical scheme for differential measurements and ISR estimation (left) and agents block scheme for the implementation of the proposed DGNSS ranging paradigm (right).

TABLE I: RVD phases with associated distances and AKEs.

Phase Name	**Distance**	**AKE**
Far Rendezvous	10000 m	5%
Inspection	1000 m	2%
Close Rendezvous	100 m	1%
Final Approach	50 m	0.02%

spacecrafts by relying on their independent observations of the GNSS pseudorange measurements. These measurements are assumed to be retrieved for the same set of visible satellites throughout the rendezvous phases of the mission. By assuming the CubeSat as reference, we refer to *chaser* and *target* pseudorange measurements to distinguish between those observables retrieved at the CubeSat and at the mothership receivers, respectively. In the context of space missions, we also refer to the estimated Euclidean distance as Inter-Spacecraft Range (ISR) to distinguish this study from similar approaches investigated in terrestrial applications [13]–[15]. RVD phases foreseen by the mission plan are provided in Table I along with the pre-defined AKE. The requirements becomes more and more stringent as the the distance between the spacecrafts decreases. Pseudorange measurements are assumed to be estimated at the mothership's GNSS receiver and transmitted through a dedicated telemetry/data link to the CubeSat. Modern inter-satellite link (ISL) may be used for line-of-sight transmission but any indirect link that can guarantee a sufficiently-low latency is also suitable, as demonstrated for terrestrial applications [15], [16]. Such a communication channel, referred to as COM in Figure 1, is hence assumed available to estimate ISRs and is fundamental for the feasibility of the presented approach. Furthermore, both the spacecraft are assumed carrying multi-constellation, multi-frequency GNSS receivers capable to provide output GNSS measurements with comparable precision (i.e., the same receiver module is assumed). Time synchronization between the spacecraft is left to the standalone GNSS time synchronization of the independent receivers [17], i.e. $\Delta t \leq 50\,\text{ns}$ RMS, and the measurement output rate is assumed to be $R_o \geq 1\,\text{Hz}$.

A. ISR algorithms

For the sake of simplicity, letters A and B are attributed to the CubeSat and the mothership respectively, and the combination of chaser and target measurements is foreseen at the CubeSat location (A). Figure 1 shows the high-level diagram of the problem geometry for the combination of multiple GNSS pseudorange measurements, and the associated block diagram on the right highlights the required input data.

1) Single Differences: By assuming to compensate for their time offset according to [18], a pair of chaser and target measurements, i.e., $\rho_A^s(t_k)$ and $\rho_B^s(t_k)$, referred to the same s-th satellite, can be linearly combined via Single Difference (SD) at a given time instant, as

$$\begin{aligned} S_{AB}^s(t_k) &= \rho_A^s(t_k) - \rho_B^s(t_k) \\ &= \Delta r_{AB}(t_k) + \Delta b_{AB}(t_k) + \Delta\xi_{AB}(t_k) \end{aligned} \tag{1}$$

where Δr_{AB} is a projection of the true distance between the receivers, Δb_{AB} (in meters) is the difference between the clock biases at the receivers clocks, and $\Delta\xi_{AB}$ is the residual error due to the sum of all the undifferenced error terms in the pseudorange measurements. By extending the computation to the whole set of available pseudoranges and adopting a matrix notation, the set of single differences can be obtained as in (2) where the left term and constitutes the set of SDs. The middle term is referred to as combination matrix, and the right term is composed by the pseudorange pairs retrieved by the receivers w.r.t. to a common s-th satellite, namely

$$\boldsymbol{\rho}_{AB}^s(t_k) = \begin{bmatrix} \rho_A^s(t_k) \\ \rho_B^s(t_k) \end{bmatrix}. \tag{3}$$

The single-differences range estimation problem can be formalized through

$$\begin{bmatrix} S_{AB}^1(t_k) \\ S_{AB}^2(t_k) \\ \vdots \\ S_{AB}^S(t_k) \end{bmatrix} \simeq \begin{bmatrix} \boldsymbol{h}_A^1(t_k) & 1 \\ \boldsymbol{h}_A^2(t_k) & 1 \\ \vdots & 1 \\ \boldsymbol{h}_A^S(t_k) & 1 \end{bmatrix} \begin{bmatrix} \boldsymbol{d}_{AB}(t_k) \\ \Delta b_{AB}(t_k) \end{bmatrix} \tag{4}$$

where $\boldsymbol{h}_u^s(t_k)$ denotes the unitary steering vector directed towards the s-th satellite from the u-th user location. Since user

$$\begin{bmatrix} S^1_{AB}(t_k) \\ S^2_{AB}(t_k) \\ \vdots \\ S^S_{AB}(t_k) \end{bmatrix} = \begin{bmatrix} -1 & 1 & 0 & 0 & \cdots & \cdots & 0 & 0 \\ 0 & 0 & -1 & 1 & \vdots & \vdots & 0 & 0 \\ \vdots & \vdots & \cdots & \cdots & \ddots & \ddots & \vdots & \vdots \\ 0 & 0 & 0 & 0 & \cdots & \cdots & -1 & 1 \end{bmatrix} \begin{bmatrix} \boldsymbol{\rho}^1_{AB}(t_k) \\ \boldsymbol{\rho}^2_{AB}(t_k) \\ \vdots \\ \boldsymbol{\rho}^s_{AB}(t_k) \end{bmatrix} \tag{2}$$

location is typically unknown, such a matrix is computed w.r.t. to an arbitrarily chosen approximation point that is iteratively updated within the estimation algorithm. By applying a Least Square (LS) algorithm, we can solve for (4) by

$$\boldsymbol{d}^{(SD)}_{AB}(t_k) \simeq \left(\boldsymbol{H}_A \boldsymbol{H}_A^T\right)^{-1} \boldsymbol{H}_A^T \boldsymbol{S}_{AB}(t_k) \tag{5}$$

where $\boldsymbol{d}^{SD}_{AB}(t_k)$ denotes the estimated ISR by means of SD. By assuming the availability at the receiver of the pseudorange measurements variances, the measurements error covariance can be considered to weight the computation of (5). The error covariance of the input measurements, $\boldsymbol{R}_{SD}$, is diagonal if the satellites are not repeated among the pairs used in single differences. A generic element of the diagonal of $\boldsymbol{R}_{SD}$ is hence defined as $[\boldsymbol{R}_{SD}]_{ss} = (\sigma^s_A)^2 + (\sigma^s_B)^2$. A weighted geometrical matrix can be hence defined as

$$\bar{\boldsymbol{H}}_A \simeq \left(\boldsymbol{H}_A^T \boldsymbol{R}_{SD}^{-1} \boldsymbol{H}_A\right)^{-1} \boldsymbol{H}_A^T \boldsymbol{R}_{SD}^{-1} \tag{6}$$

and $\bar{\boldsymbol{H}}_A$ can be replaced in (5) to perform a weighted estimate of $\boldsymbol{d}^{(SD)}_{AB}(t_k)$. When unweighted LS is considered, the output covariance associated to the range estimate can be computed as

$$\boldsymbol{R}_d^{(SD)} = \left(\boldsymbol{H}_A^T \boldsymbol{H}_A\right)^{-1} \boldsymbol{H}_A^T \boldsymbol{R}_{SD} \boldsymbol{H}_A \left(\boldsymbol{H}_A^T \boldsymbol{H}_A\right)^{-1}. \tag{7}$$

In case WLS is exploited and the weighting matrix is the inverse of the input error covariance, the output error covariance simplifies to $\boldsymbol{R}_d^{(SD)} = \left(\boldsymbol{H}_A^T \boldsymbol{R}_{SD}^{-1} \boldsymbol{H}_A\right)^{-1}$.

2) Double Differences: Regarding Double Differences (DD), we can exploit the same steps as for SDs, by computing each DD as a difference of SDs

$$D^{ij}_{AB}(t_k) = S^j_{AB}(t_k) - S^i_{AB}(t_k) = \Delta R_{AB}(t_k) + \Sigma_{AB}(t_k) \tag{8}$$

where ΔR_{AB} is the actual difference between SDs, and $\Sigma_{AB}(t_k)$ collects all the non-mutual residual errors that cannot cancel out. By extending the number of measurements through a matrix notation, as in (4), we set up the linear combination of all the available single differences, as

$$\begin{bmatrix} D^{12}_{AB}(t_k) \\ D^{13}_{AB}(t_k) \\ \vdots \\ D^{1S}_{AB}(t_k) \end{bmatrix} = \begin{bmatrix} -1 & 1 & 0 & \cdots & 0 \\ -1 & 0 & 1 & 0 & \vdots \\ \vdots & \vdots & \ddots & \ddots & 0 \\ -1 & 0 & \cdots & 0 & 1 \end{bmatrix} \begin{bmatrix} S^1_{AB}(t_k) \\ S^2_{AB}(t_k) \\ \vdots \\ S^S_{AB}(t_k) \end{bmatrix} \tag{9}$$

where the left term collects all the DDs, the middle term describe the algebraic combination matrix, and the right term is computed through (4). The double difference range vector estimation is hence achieved, by inverting

$$\begin{bmatrix} D^{12}_{AB}(t_k) \\ D^{13}_{AB}(t_k) \\ \vdots \\ D^{1S}_{AB}(t_k) \end{bmatrix} \simeq \begin{bmatrix} \boldsymbol{h}^2_A(t_k) - \boldsymbol{h}^1_A(t_k) \\ \boldsymbol{h}^2_A(t_k) - \boldsymbol{h}^1_A(t_k) \\ \vdots \\ \boldsymbol{h}^S_A(t_k) - \boldsymbol{h}^1_A(t_k) \end{bmatrix} \boldsymbol{d}_{AB}(t_k). \tag{10}$$

By propagating the single differences' measurements error covariance defined in (7) through the DD ranging derivation, we obtain

$$\bar{\boldsymbol{H}}_D \simeq \left(\boldsymbol{H}_A^T \left(\boldsymbol{R}_d^{(SD)}\right)^{-1} \boldsymbol{H}_A\right)^{-1} \boldsymbol{H}_A^T \left(\boldsymbol{R}_d^{(SD)}\right)^{-1} \tag{11}$$

and eventually, the range vector estimate is obtained through LMS estimation of

$$\boldsymbol{d}^{(DD)}_{AB}(t_k) \simeq \bar{\boldsymbol{H}}_D \boldsymbol{D}_{AB}(t_k) \tag{12}$$

where $\boldsymbol{d}^{(DD)}_{AB}(t_k)$ denotes the estimated ISR by means of DD. In case of unweighted LS, the associated error covariance, is hence

$$\boldsymbol{R}_d^{(DD)} = \left(\boldsymbol{H}_D^T \boldsymbol{H}_D\right)^{-1} \boldsymbol{H}_D^T \boldsymbol{R}_d^{(SD)} \boldsymbol{H} \left(\boldsymbol{H}_D^T \boldsymbol{H}_D\right)^{-1}. \tag{13}$$

In case WLS is exploited and the weighting matrix is the inverse of the input error covariance, the output error covariance simplifies to $\boldsymbol{R}_d^{(DD)} = \left(\boldsymbol{H}_D^T \left(\boldsymbol{R}_d^{SD}\right)^{-1} \boldsymbol{H}_D\right)^{-1}$. SD (`Al_01`), DD (`Al_02`) and a variant of the latter (`Al_03`) that was introduced in [19], were tested in the current analysis. It is worth remarking that, under the assumptions of i.i.d. input measurements with standard deviation σ_u, SDs are characterized by a standard deviation equal to $\sqrt{2}\sigma_u$. DDs (`Al_02`, `Al_03`) are in turn characterized by a standard deviation of $2\sigma_u$. Shortly, while common biases cancel out, pseudorange/range measurements noise is increased by differentiation. This may lead to a higher uncertainty in the relative positioning when compared to absolute positions difference but it keeps ISR estimates fully independent of any state estimator. It is worth remarking that a standard deviation, σ_d, of the output ISR estimate cannot be computed in closed form from non-diagonal output covariance matrices [20], as in the case of (7) and (13). Therefore, a simulation environment was required for an exhaustive characterization of such an uncertainty under different variances on the input measurements.

B. Simulation Environment

Input data from an STK mission simulation includes:

- GPS/Galileo Constellation STK reports: includes state space and velocity of the GNSS satellites at the mission time

- CubeSat (chaser) and mothership (target) STK Reports: include state space and velocity of the spacecrafts at the mission time
- GPS/Galileo to mothership/CubeSat STK access report: include the GNSS satellites visible in Line-of-Sight (LoS) to the spacecrafts

Space state coordinates are intended in ICRF reference frame. However, the choice of the ICRF frame does not imply a lack of generality. ISR computation is invariant w.r.t. the selected reference frame and the following simulation architecture holds for any Cartesian system. Spacecraft's sate space and velocity data was provided by means of the STK report. The time granularity for the generation of the report was set to 30 s. A file parser and a subroutine for the tracking of visible GNSS satellites at each time instant was implemented and a dedicated function was designed to inject the User Equivalent Range Error (UERE) noise [21] to the exact satellite-user ranges. A dedicated routine included the ranging algorithms described in Section II-A and an Iterative Least Mean Square (I-LMS) routine for the ML estimation of (5) and (12), for SD and DD respectively. Both measurements simulation and ISR estimation routines are embedded in a Monte Carlo environment to support a statistical analysis of the estimated ISRs by randomizing the noise generation. Parametric Monte Carlo simulations were performed to characterize the output statistics by varying the UERE variance of the input pseudorange measurements. The Monte Carlo simulation environment was configured according to the parameters reported in Table II.

III. Results and Discussion

As a preliminary investigation, the actual mission trajectories and visibility constraints about GNSS satellites were not considered to prevent unrealistic assumptions on the geometrical dilution of precision [21].

A. Numerical analysis of the estimation bias

By setting the standard deviation of each input measurements to $\sigma_u = 0\,\text{m}$ (noiseless input measurements), and observing the two spacecraft approaching from very large distances, biased ISR estimates appear for all the three DGNSS methods. Estimation biases decrease below the $0.001\,\%$ of the true baseline length for all the methods, e.g., returning bias values lower than $50\,\text{m}$ at $50\,\text{km}$ of distance and lower than $5\,\text{cm}$ at $5\,\text{m}$. By only accounting for the algorithmic bias, we assessed that, under ideal assumptions, the algorithms can guarantee an error that is lower than the minimum AKE imposed by the mission for the close rendezvous phase, i.e., $< 0.02\,\%$ of the true distance. Such an intrinsic bias has to be attributed to unsuitable geometrical assumptions on the parallelism of the steering vectors done for (4) and (10) that looses validity with the distance between the spacecrafts [19]. A complementary, statistical analysis in more realistic conditions is presented hereafter.

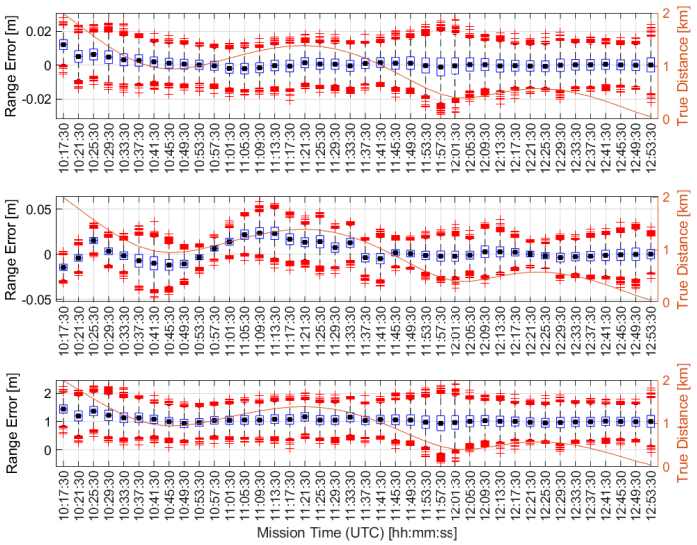

(a) $\sigma_u = 0.01\,\text{m}$

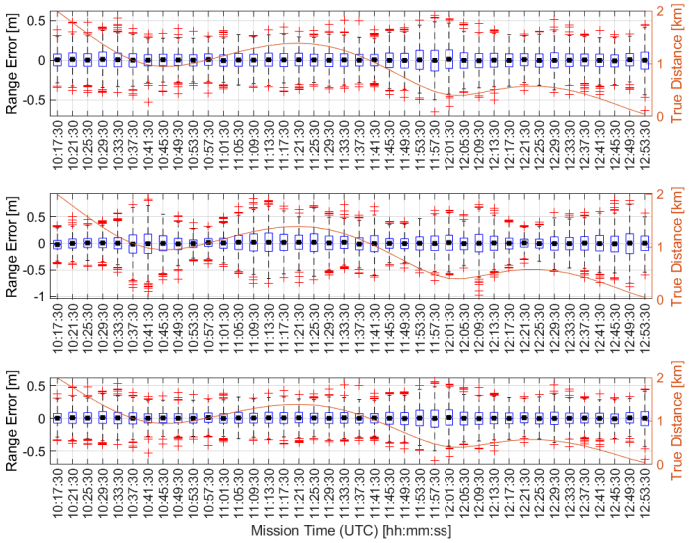

(b) $\sigma_u = 0.25\,\text{m}$

Fig. 2: Statistical characterization of the estimated ISR for different UERE standard deviations. UTC time is referred to a simulated SROC mission trajectory.

B. ISR simulation considering actual GNSS visibility

A pair of sample results from the overall Monte Carlo analysis are reported and discussed hereafter. ISR accuracy and precision analysis for the selected ranging algorithms are reported in form of box plots in Figures 2a and 2b for $\sigma_u = 0.01\,\text{m}$ and $\sigma_u = 0.25\,\text{m}$, respectively. The algorithms are distinguished by upper (`Al_01`), middle (`Al_02`), and lower (`Al_03`) subplots. Each subplot shows a box plot describing a summary statistics of the ISR for the Monte Carlo output observed every $240\,\text{s}$ of the mission timespan (time-decimated w.r.t. to the granularity of the STK reports). The box plots show a summary statistics of the sample data.

TABLE II: **Configuration parameters of the MATLAB Simulation Environment**

Parameter	**Value**
User Equivalent Range Error Standard Deviation, σ_u	$[0.01, 0.10, 0.50, 2.00, 10.00]$ m
Number of Monte Carlo trials	> 5000 (up to convergence)
Mission Time (and associated A-B distance)	10:05:00 – 12:57:00 UTCG (2 km – 0 km)
Iterative LMS (I-LMS) iterations	10

The bottom and top of each blue box are the 25th and 75th percentiles of the sample, respectively. The distance between the bottom and top of each box is the interquartile range. The black square inside the box identifies the sample mean. The whiskers are lines extending above and below each box going from the end of the interquartile range to the furthest observation within the whisker length. Observations beyond the whisker length are identified as outliers and marked with red markers. Outliers are significant to a conservative analysis on the observed uncertainties. The box plot statistics is referred to the left y-axis (range error). The overlapping orange curve is the true distance between mothership and CubeSat according to the STK simulation environment. The curve is referred to the right y-axis and spans in the range 2-0 km. Overall, it can be observed that `Al_01` and `Al_02` have similar statistical behaviours, with a lower sensitivity to the ISR variations along the mission trajectory and RVD phases. A strong correlation between bias and true distance is instead notable for `Al_02` in 2a that is hidden by larger error statistics in the experiments of Figure 2b. A remarkable correlation between standard deviation and ISR variations is similarly visible for `Al_02` as tracked by whiskers and outliers of the middle subplots in Figure 2b. `Al_02` provides estimation errors with a less stable behaviour of their statistical distribution that has not be attributable to the variable geometry of the observed GNSS constellations. `Al_02` is hence not appropriate to be considered for the integration of ISR in fused GNC solutions for relative navigation.

C. Time-aggregated metrics for ISR error modelling

To provide a suitable model for the integration of the ISR measurements into a relative navigation filter, the following tables provide time-aggregated metrics affecting the ISR error for an extended range of values of σ_u. Minimum, maximum and mean estimation bias and standard deviation experienced along the mission trajectories are provided in Figures 3a and 3b, respectively. Statistics have been obtained through sample mean and variance evaluated through the whole output sample space of the Monte Carlo trials. In Figure 3a, the error bias is always lower than 1 m and it can be assumed lower than 0.1 m when carrier-smoothed pseudorange are considered. Output standard deviation in Figure 3b shows a linear relationship with the input σ_u (i.e., logarithmic relationship into logarithmic scale).

D. Uncertainty bound for ISR integration in navigation filters

Both mothership and CubeSat are supposed to host a NOVATEL OEM719 GNSS space-born receiver for multi-constellation, multi-frequency GNSS navigation in space applications. It hosts 555 channels, providing measurements at a maximum output rate of 100 Hz, and a declared time RMS accuracy of 20 ns. The receiver can provide code measurements with a maximum precision of 0.08 m and carrier-smoothed measurements with a worst-case precision of 0.001 m [22]–[24]. As a conservative approach w.r.t. to the commercial datasheet provided by the manufacturer, we bounded the overall UERE standard deviation, σ_u, to 0.01 m by assuming a margin of one order of magnitude for the input measurements error. The values of bias and standard deviation included in Figures 3a and 3b can be used to retrieve ISR measurements statistics for the selected input UERE (i.e., 0.01 m) and to identify an overall conservative bound for their further integration. Worst case statistics are shown in second and third column of Table III for all the three proposed DGNSS methods. The fourth column provides a conservative 3σ-bound that treats intrinsic biases as isotropic uncertainties and sum them up to worst case standard deviation, according to

TABLE III: Summary of worst case statistics observed for the different DGNSS methods, considering $\sigma_u = 0.01$ m and including conservative 3σ-bound, Σ_d .

Algorithm	$3\sigma_d$ (std. dev. [m])	μ_d (bias [m])	Σ_d [m]
`Al_01`	0.0801	0.01	0.10
`Al_02`	0.036	0.0082	0.06
`Al_03`	0.00279	0.0082	0.05

$$\Sigma_d = \alpha(3\sigma_d + \mu_d) \tag{14}$$

where $\alpha = 1.3$ provides an additional guard uncertainty of the $30\,\%$ that is designed and applied to the combined boundary statistics to include unmodelled error sources.

This approach enlarges the uncertainty for any dimension of a three-dimensional reference frame thus producing a highly-conservative, direction-independent bound of the measurement uncertainty. The recommended σ_d^+ can be used to initialize input error covariance matrices in Bayesian estimation filters such as Extended Kalman Filter.

IV. Conclusions

Fundamental DGNSS techniques such as single and double differences can complement other ranging solutions for small-scale satellites such as CubeSat. This paper investigates the usability of such fundamental techniques in RVD manoeuvres between GNSS-equipped LEO chaser and target. According

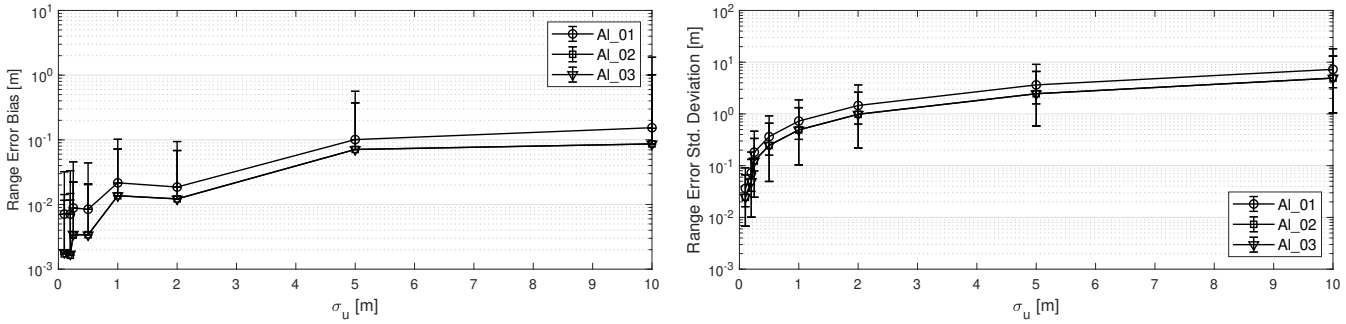

(a) (b)

Fig. 3: Mean values of ISRs bias (a) and standard deviation (b) shown in logarithmic scale with maximum and minimum (whiskers) as observed throughout the full mission timespan by varying the input UERE with $\sigma_u \in (0.1, 10)$ m.

to the declared performance of the reference GNSS receiver selected for this study (i.e., Novatel OEM917) and to the STK mission simulation, the recommended, conservative standard deviation values are 0.10 m for algorithm `Al_01` (SD) and 0.05 m for `Al_03` (DD). Such boundaries are determined by assuming input measurements noise with $\sigma_u = 0.001$ m that is compatible with carrier-smoothed pseudorange measurements.

REFERENCES

[1] F. Bauer, M. Moreau, M. Dahle-Melsaether, W. Petrofski, B. Stanton, S. Thomason, G. A. Harris, R. Sena *et al.*, "The GPS space service volume," in *Proceedings of the 19th international technical meeting of the Satellite Division of the Institute of Navigation (ION GNSS 2006)*, 2006, pp. 2503–2514.

[2] R. Kroes, O. Montenbruck, W. Bertiger, and P. Visser, "Precise GRACE baseline determination using GPS," *Gps Solutions*, vol. 9, no. 1, pp. 21–31, 2005.

[3] F. Stesina, "Tracking model predictive control for docking maneuvers of a cubesat with a big spacecraft," *Aerospace*, vol. 8, no. 8, 2021. [Online]. Available: https://www.mdpi.com/2226-4310/8/8/197

[4] F. Stesina, S. Corpino, C. Novara, and S. Russo, "Docking manoeuvre control for cubesats," *The Journal of the Astronautical Sciences*, vol. 69, no. 2, pp. 312–334, 2022.

[5] S. Corpino and F. Stesina, "Inspection of the cis-lunar station using multi-purpose autonomous cubesats," *Acta Astronautica*, vol. 175, pp. 591–605, 2020.

[6] S. Corpino, F. Stesina, D. Calvi, and L. Guerra, "Trajectory analysis of a cubesat mission for the inspection of an orbiting vehicle," *Advances in aircraft and spacecraft science*, vol. 7, no. 3, pp. 271–290, 2020.

[7] L. Sun, J. Yang, W. Huang, L. Xu, S. Cao, and H. Shao, "Inter-satellite time synchronization and ranging link assignment for autonomous navigation satellite constellations," *Advances in Space Research*, vol. 69, no. 6, pp. 2421–2432, 2022.

[8] P. Chen, L. Shu, R. Ding, and C. Han, "Kinematic single-frequency relative positioning for LEO formation flying mission," *GPS Solut.*, vol. 19, no. 4, p. 525–535, oct 2015.

[9] D. Gu, B. Ju, J. Liu, and J. Tu, "Enhanced GPS-based GRACE baseline determination by using a new strategy for ambiguity resolution and relative phase center variation corrections," *Acta Astronautica*, vol. 138, pp. 176–184, 2017, the Fifth International Conference on Tethers in Space.

[10] C. Zhang, D. Dong, W. Chen, M. Cai, Y. Peng, C. Yu, and J. Wu, "High-accuracy attitude determination using single-difference observables based on multi-antenna GNSS receiver with a common clock," *Remote Sensing*, vol. 13, no. 19, 2021. [Online]. Available: https://www.mdpi.com/2072-4292/13/19/3977

[11] S. Corpino, G. Ammirante, G. Daddi, F. Stesina, F. Corradino, A. Basler, A. Francesconi, F. Branz, J. Van den Eynde *et al.*, "Space Rider Observer Cube–SROC: a CubeSat mission for proximity operations demonstration," in *Proc. 73rd International Astronautical Congress (IAC)*, 2022.

[12] A. Minetto, G. Falco, and F. Dovis, "On the trade-off between computational complexity and collaborative GNSS hybridization," in *2019 IEEE 90th Vehicular Technology Conference (VTC2019-Fall)*, 2019, pp. 1–5.

[13] A. Minetto, A. Nardin, and F. Dovis, "GNSS-only collaborative positioning among connected vehicles," in *Proceedings of the 1st ACM MobiHoc Workshop on Technologies, MOdels, and Protocols for Cooperative Connected Cars*, ser. TOP-Cars '19. New York, NY, USA: Association for Computing Machinery, 2019, p. 37–42. [Online]. Available: https://doi.org/10.1145/3331054.3331552

[14] F. Wang, W. Zhuang, G. Yin, S. Liu, Y. Liu, and H. Dong, "Robust inter-vehicle distance measurement using cooperative vehicle localization," *Sensors*, vol. 21, no. 6, p. 2048, 2021.

[15] F. Raviglione, S. Zocca, A. Minetto, M. Malinverno, C. Casetti, C. Chiasserini, and F. Dovis, "From collaborative awareness to collaborative information enhancement in vehicular networks," *Vehicular Communications*, vol. 36, p. 100497, 2022.

[16] A. Minetto, M. C. Bello, and F. Dovis, "DGNSS cooperative positioning in mobile smart devices: A proof of concept," *IEEE Transactions on Vehicular Technology*, vol. 71, no. 4, pp. 3480–3494, 2022.

[17] K. F. Hasan, Y. Feng, and Y.-C. Tian, "GNSS time synchronization in vehicular ad-hoc networks: Benefits and feasibility," *IEEE Transactions on Intelligent Transportation Systems*, vol. 19, no. 12, pp. 3915–3924, 2018.

[18] F. de Ponte Müller, E. M. Diaz, B. Kloiber, and T. Strang, "Bayesian cooperative relative vehicle positioning using pseudorange differences," in *2014 IEEE/ION Position, Location and Navigation Symposium-PLANS 2014*. IEEE, 2014, pp. 434–444.

[19] A. Delépaut, A. Minetto, F. Dovis, F. Melman, P. Giordano, and J. Ventura-Traveset, "Enhanced GNSS-based positioning in space exploiting inter-spacecraft cooperation," in *Proceedings of the 2022 International Technical Meeting of The Institute of Navigation*, 2022, pp. 530–544.

[20] S. Zocca, A. Minetto, and F. Dovis, "Adaptive Bayesian state estimation integrating non-stationary DGNSS inter-agent distances," in *2021 IEEE 93rd Vehicular Technology Conference (VTC2021-Spring)*, 2021, pp. 1–7.

[21] E. D. Kaplan and C. Hegarty, *Understanding GPS/GNSS: Principles and applications*. Artech house, 2017.

[22] N. Inc., "Novatel oem719 performance specifications," https://docs.novatel.com/OEM7/Content/Technical-Specs-Receiver/OEM719-Performance-Specs.htm, 2022 (accessed May 5, 2023).

[23] ——, "Carrier smoothing configuration," 2022 (accessed December 7, 2014).

[24] S. Boyd and L. Vandenberghe, *Introduction to applied linear algebra: vectors, matrices, and least squares*. Cambridge university press, 2018.